


Absorbance enhancement of monolayer MoS₂ in a perfect absorbing systemXia Zhang¹,* Julia Lawless¹,* Jing Li, John F. Donegan, and A. Louise Bradley¹†
*School of Physics, CRANN and AMBER, Trinity College Dublin, Dublin 2, Ireland*Lisanne Peters¹ and Niall McEvoy
School of Chemistry and AMBER, Trinity College Dublin, Dublin 2, Ireland (Received 22 December 2021; accepted 7 April 2022; published 29 April 2022)

We reveal numerically and experimentally that dielectric resonances can enhance the absorbance and emission of monolayer MoS₂. By quantifying the absorbance of the Si disk resonators and the monolayer MoS₂ separately, a model taking into account the absorbance as well as quantum efficiency modifications by the dielectric disk resonators successfully explains the observed emission enhancement under normal light incidence. It is demonstrated that the experimentally observed emission enhancement at different pump wavelength results from the absorbance enhancement, which compensates the emission quenching by the disk resonators. In order to further maximize the absorbance value of monolayer MoS₂, a perfect absorbing structure is proposed. By placing a Au mirror beneath the Si nanodisks, the incident electromagnetic power is fully absorbed by the hybrid monolayer-MoS₂-disk system. It is demonstrated that the electromagnetic power is redistributed within the hybrid structure and 53% of the total power is absorbed by the monolayer MoS₂ at the perfect absorbing wavelength.

DOI: [10.1103/PhysRevMaterials.6.045202](https://doi.org/10.1103/PhysRevMaterials.6.045202)**I. INTRODUCTION**

Tailoring the absorbance and emission properties of an emitter is of great interest in terms of both understanding the fundamental physics and the application prospects [1]. Both are determined by the electromagnetic environment of the emitter, which can be realized by positioning the emitter in the near field of a resonant cavity, such as a photonic-crystal nanocavity [2–4], plasmonic nanoantenna [5,6], or grating [7,8]. Particularly, both properties are fundamentally correlated. The Purcell effect describes the modification of the spontaneous emission rate due to the emitter's environment through the refractive index, and the resonator mode volume and quality factor [9]. The spontaneous emission can also be modified by the absorbance enhancement. Such absorbance and emission tailoring belong to the regime of weak light-matter coupling, or the perturbative regime. Monolayer two-dimensional (2D) transition metal dichalcogenides (TMDCs) have become core materials for nanoscale devices due to reduced dimensionality, ease of integration, and advanced optical and electronic functionalities, such as nanolaser [10], photodetector [11], and nonlinear optic elements [12].

Monolayer TMDCs exhibit a direct band gap at visible and near-infrared wavelengths [13]. However, due to the atomic thickness of the layer and following the Beer-Lambert absorbance law, low optical absorbance and emission of monolayer TMDCs pose an obstacle for conversion of pho-

ton energy into other forms of energy. Intensive efforts have therefore been devoted to enhance the absorbance or emission of monolayer TMDCs, such as by employing a photonic crystal slab backed by a perfect electric conductor mirror [14], a multilayer photonic structure including a dielectric grating, a spacer, and a metal film [15], and a sandwiched photonic crystal slab with air holes and a silver mirror [16] or through a metasurface [17], photonic hypercrystals [18], a photonic Fano resonance [19], and a plasmonic antenna [20,21]. The maximum absorbance that a structure can achieve is 1, referred to as a perfect absorber or coherent perfect absorption (CPA) [22,23]. CPA can involve interference due to two or more input waves including counterpropagating input waves and can be manipulated by varying the relative phase of the two inputs [23]. Due to its versatile manipulation, such configurations are useful for applications in modulators and optical switches.

In this paper, we demonstrate experimentally that Si nanodisk resonators are capable of confining the energy within monolayer MoS₂ to achieve absorbance enhancement. The signature of absorbance enhancement via increased emission is experimentally observed. The emission enhancement as well as the absorbance of monolayer MoS₂ are quantified and agree with the experimental observation. Based on this, we further explore the use of a mirror to increase the absorbance of monolayer MoS₂, wherein a perfect absorbing system is proposed enabling more than 50% of the total power to be absorbed by the monolayer MoS₂.

II. EXPERIMENT AND MODEL

A schematic of the hybrid emitter-resonator structure can be seen in Fig. 1, which shows the MoS₂ monolayer

*These authors contributed equally to this work.

†bradl@tcd.ie

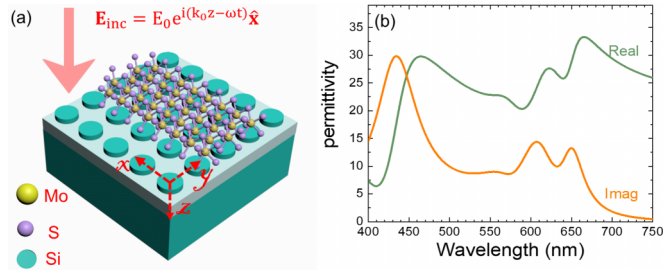


FIG. 1. (a) Schematic of the hybrid Si nanodisk metasurface and monolayer MoS₂ on SiO₂/Si substrate. A normally incident plane wave propagates along the z direction and is polarised along the x direction, $\mathbf{E}_{\text{inc}} = E_0 e^{i(k_0 z - \omega t)} \hat{x}$. (b) The real and imaginary (Imag) components of the dielectric permittivity of monolayer MoS₂.

on the Si nanodisk resonators, sitting on a SiO₂/Si substrate. The permittivity of monolayer MoS₂ is taken from Ref. [24] and is shown in Fig. 1(b). The Si nanodisk metasurface is fabricated on a Si-on-insulator (SOI) wafer (45 nm top Si thickness, 150 nm buried oxide thickness; Soitec). Electron-beam (e-beam) lithography was performed on a spin-coated poly(methyl methacrylate) (PMMA) 950 layer (A3, 3000 rpm) by electron beam (Elionix ELS 7700), followed by development in methyl isobutyl ketone–isopropyl alcohol (MIBK-IPA) at a ratio of 1 : 3. A 20-nm-thick chromium (Cr) layer was deposited by e-beam evaporator (Temescal). After the lift-off process in hot Remover 1165, the Cr layer was used as a hard mask, and the pattern was transferred to the SOI substrate by inductively coupled plasma (ICP) etching through the top Si layer, resulting in a (10 ± 3) -nm-thick buried thermal oxide (BOX) layer being etched over, verified by ellipsometry. The thickness of SiO₂ is 140 nm. The Cr mask was finally removed using a commercial Cr etchant from Sigma. The scanning electron microscope images and Raman and photoluminescence (PL) maps of the fabricated hybrid sample are shown in Fig. 2(a) for disk radius $r = 160$ nm and period $p_x = p_y = 500$ nm. The experimental measurement details, including reflectance spectra and Raman spectra, proving the monolayer nature of MoS₂ can be found in the Supplemental Material [25]. As can be seen in Figs. 2(b) and 2(c), the measured emission intensity displays an enhancement due to the presence of the nanodisk resonators at excitation wavelengths of both $\lambda_{\text{ex}} = 405$ nm and $\lambda_{\text{ex}} = 532$ nm. The PL enhancements, defined as η , at both pump wavelengths, denoted as red dashed lines, are shown in Fig. 2(d).

In order to investigate the physics driving the PL enhancement, a model linking absorbance and emission is required. Following the law of power conservation, the sum of reflectance, transmittance, and absorbance is unity. Therefore the absorbance A is typically determined as [21]

$$A = 1 - R - T, \quad (1)$$

where R and T represent the reflectance and transmittance, respectively. Equation (1) offers a flexible way, numerically and experimentally, to quantify the absorbance value of the hybrid structure or separate components. However, in the hybrid sample, aiming for the quantification of the absorbance of the constituting elements, such as the monolayer MoS₂ or

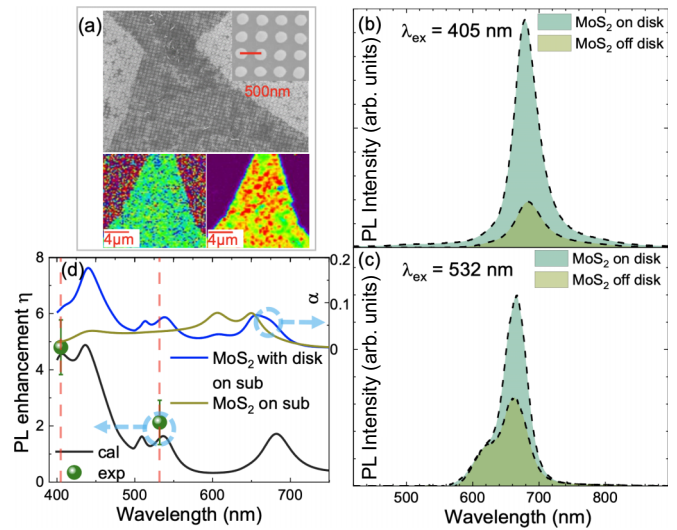


FIG. 2. (a) Scanning electron microscope images (top) and Raman (bottom left) and PL (bottom right) maps of the fabricated hybrid MoS₂-Si-nanodisk sample on SiO₂/Si substrate for radius $r = 160$ nm. (b) and (c) Experimentally measured PL spectra of monolayer MoS₂, on disk and off disk, with the excitation wavelengths of $\lambda_{\text{ex}} = 405$ nm (b) and $\lambda_{\text{ex}} = 532$ nm (c), denoted as vertical dashed lines in (d). (d) At top, with y-axis values shown on the right: the calculated absorbance α of monolayer MoS₂ on a SiO₂/Si substrate (sub) and that hybridized with Si disks on a SiO₂/Si substrate. At bottom, with y-axis values shown on the left: the experimentally measured and calculated PL enhancement η .

the Si nanodisk, it is critical to separate the power dissipation within the disk and that within the monolayer MoS₂. The absorbance of a nanostructure, here the monolayer MoS₂ or the disk metasurface, is the ratio of the total absorbed power within a volume V (P_{abs}) to the incoming power over the exposed surface area S_0 [26,27]; the absorbance under normal incidence can also be calculated analytically as

$$\alpha = \frac{P_{\text{abs}}}{P_{\text{inc}}} = \frac{k_0}{S_0 |E_0|^2} \iiint_V \text{Im}[\epsilon(\mathbf{r})] |\mathbf{E}(\mathbf{r})|^2 dV, \quad (2)$$

where $P_{\text{abs}} = \frac{1}{2} c \epsilon_0 k_0 \iiint_V \text{Im}(\epsilon) |\mathbf{E}(\mathbf{r})|^2 dV$ [15,28]. $|\mathbf{E}(\mathbf{r})|$ is the amplitude of the electric field within the monolayer of MoS₂ or the Si disk resonators. ϵ is the corresponding dielectric permittivity. The integration is performed in one unit cell over the volume V , and $V = p_x \times p_y \times h(t_0)$, where h and t_0 denote the height of the disk and the thickness of the MoS₂ monolayer, respectively. P_{inc} denotes the incident source power calculated over one unit cell in free space, $P_{\text{inc}} = \frac{1}{2} c \epsilon_0 S_0 |E_0|^2$. k_0 is the free-space wave vector, and c is the free-space light speed. S_0 is the area of one unit cell, $S_0 = p_x \times p_y$. $|E_0|$ is the electric field amplitude of the incident light, which is $\mathbf{E}_{\text{inc}} = E_0 e^{i(k_0 z - \omega t)} \hat{x}$. Equation (1) is used to calculate A , the absorbance of a structure, which can be either the complete hybrid structure or the bare metasurface or the monolayer in the absence of the metasurface. In contrast, α is used to quantify the absorbance of each component within the complete hybrid structure. A detailed discussion of the absorbance determination for periodic structures can be found elsewhere [29].

As can be seen from the curves plotted at the top of Fig. 2(d), which show the absorbance of monolayer MoS₂, α is enhanced due to the influence of disk resonators at 405 and 532 nm, indicated as vertical dashed lines. The absorbance enhancement at different pump wavelengths is quantified as the ratio of the absorbance of monolayer MoS₂ on disk to that off disk as $\alpha(\lambda_{\text{pump}})/\alpha^0(\lambda_{\text{pump}})$. Furthermore, as well as the effect of the Si nanodisk on the absorbance, the effect on the quantum efficiency needs to be considered. The MoS₂ monolayer can be represented as an array of in-plane dipoles, and the decay rates can be described by a simplified two-level quantum approach. The excitonic population relaxation rate γ_{ex} includes the radiative part $\gamma_{\text{ex}}^{\text{r}}$ and the nonradiative part $\gamma_{\text{ex}}^{\text{nr}}$ as $\gamma_{\text{ex}} = \gamma_{\text{ex}}^{\text{r}} + \gamma_{\text{ex}}^{\text{nr}}$. The quantum efficiency of the quantum system is $q = \gamma_{\text{ex}}^{\text{r}}/(\gamma_{\text{ex}}^{\text{r}} + \gamma_{\text{ex}}^{\text{nr}})$. The effective PL enhancement factor η is quantified as [6,30]

$$\eta = \frac{\alpha(\lambda_{\text{pump}})}{\alpha^0(\lambda_{\text{pump}})} \cdot \frac{q(\lambda_{\text{em}})}{q^0(\lambda_{\text{em}})}, \quad (3)$$

where $\alpha(\lambda_{\text{pump}})$ and $\alpha^0(\lambda_{\text{pump}})$ represent the absorbance of the MoS₂ monolayer at the pump wavelength on disk and off disk, respectively. $q(\lambda_{\text{em}})$ and $q^0(\lambda_{\text{em}})$ represent the quantum efficiency at the peak emission wavelength of the MoS₂ monolayer in the hybrid structure on the Si disk and of the MoS₂ monolayer off disk, respectively. The quantum efficiency is calculated at the peak emission wavelength $\lambda_{\text{em}} = 673$ nm.

All the calculations are performed by commercial finite-difference time-domain (FDTD) software (FDTD; Lumerical Solutions). In the calculation, including R , T , A , and P_{abs} , a linearly polarized, normally incident plane-wave source is applied, $\mathbf{E}_{\text{inc}} = E_0 e^{i(kz - \omega t)} \hat{\mathbf{x}}$. Periodic boundary conditions are applied in the x - y directions with pitch $p_x = p_y = 500$ nm. A perfectly matched layer boundary condition is employed in the z direction. The monolayer MoS₂ is modeled as a thin sheet of thickness of 0.75 nm, with the permittivity of MoS₂ [24]. The numerically simulated reflectance spectra match with the experimentally measured curves, which can be found in the Supplemental Material [25]. For the quantum efficiency calculation, the monolayer MoS₂ can be treated as a point dipole emitter due to its subwavelength exciton coherence length and ~ 1 nm exciton Bohr radius [19,31,32]. The quantum efficiency calculation is averaged over 11 different positions relative to the nanodisk resonator within one unit cell. The detailed calculation can be seen in the Supplemental Material [25]. The origin of the coordinate vector is placed at the center of the nanodisk. The dipole positions for the simulations are as follows: x_0 ranges from 0 to 500 nm in steps of 50 nm; $y_0 = 0$; and $z_0 = (h + t_0)/2 = 22.875$ nm, where $h = 45$ nm for the disk height and $t_0 = 0.75$ nm for the measured thickness of the monolayer MoS₂. The dipole is oriented parallel to the substrate surface. A value of 0.74 is obtained for the ratio $q(\lambda_{\text{em}})/q^0(\lambda_{\text{em}})$, which indicates that the presence of the substrate results in the emission quenching of the MoS₂ monolayer. However, the absorbance enhancement compensates the losses. As can be seen in Fig. 2(d) for disk radius of $r = 160$ nm, the calculated PL enhancement η following Eq. (3) shows agreement with the experimentally measured data, which validates our model. It also demonstrates that

the observed emission enhancement mainly arises from the absorbance enhancement.

III. PERFECT ABSORBER: MIRROR EFFECT

Absorbance enhancement has been realized using the Si disk resonators on SiO₂/Si substrate; however, the absorbance value is still quite low, especially at the A exciton peak. In this section, we aim to increase the absorbance value employing the substrate effect. For a clear physical picture of the effect of the substrate, the calculated absorbance spectra of the hybrid disk–MoS₂ monolayer embedded in air medium, sitting on SiO₂/Si substrate, and sitting on SiO₂/Au can be seen in Fig. 3. The inspected wavelength at 646 nm is indicated by the vertical dashed line. It can be seen that the absorbance value of monolayer MoS₂ without disk resonators is below 10% in all cases (5.7% in air, 9.5% on SiO₂/Si, and 4.6% on SiO₂/Au). Due to the resonance effect producing an enhanced electric field with the nanodisks, the absorbance of monolayer MoS₂ is enhanced at 646 nm (30% in air, 12.7% on SiO₂/Si, and 53% on SiO₂/Au).

Furthermore, the reflectance and transmittance as well as the absorbance spectra of the hybrid structures are also shown, where R and T are obtained by FDTD simulation and A is calculated by Eq. (1). Clearly, as seen from Fig. 3(c), the whole structure becomes a perfect absorber at the inspected wavelength ($A = 1$). Due to the mirror effect contributed by the gold plane, the transmittance becomes zero, and Eq. (1) becomes $A = 1 - R$. The electric field maps are shown at the inspected wavelength for all three cases, where the electromagnetic energy is confined inside or in the near field of the nanodisk resonator. The SiO₂/Si substrate yields the lowest field amplitude, which results from the loss due to the Si substrate. A much larger electric field amplitude is obtained for the hybrid structure on a SiO₂/Au substrate. In particular, at the position of the monolayer MoS₂ shown by the gray dashed lines, an obvious field concentration is seen compared with the hybrid structure suspended in air or on the SiO₂/Si substrate. This field concentration drives the large absorbance value of monolayer MoS₂. CPA has been observed in other systems where perfect absorbance is achieved when the scattered components interfere destructively [14,22,23]. Here, in the proposed structure on the SiO₂/Au substrate, the gold mirror reflects the transmitted wave through the hybrid structure producing destructive interference in reflection and enhanced absorbance.

It is interesting to explore further which multipolar modes of the Si nanodisk resonators drive the resonant absorbance enhancement. According to Refs. [33,34], the amplitude of decomposed multipolar modes contributing to the reflectance or transmittance coefficients is calculated by integrating the generated electric field \mathbf{E} inside the nanodisk resonators for the array, including structures suspended in air or on substrates. The substrate effect on the reflectance spectra has been experimentally and theoretically explored in Ref. [34], where the array of Si nanodisk resonators can be considered as a decoupled in-line optical element, where the modified generated electric field within the disk resonators due to the substrate needs to be taken into account. It is clear from Fig. 4 that the total electric dipole, including the electric

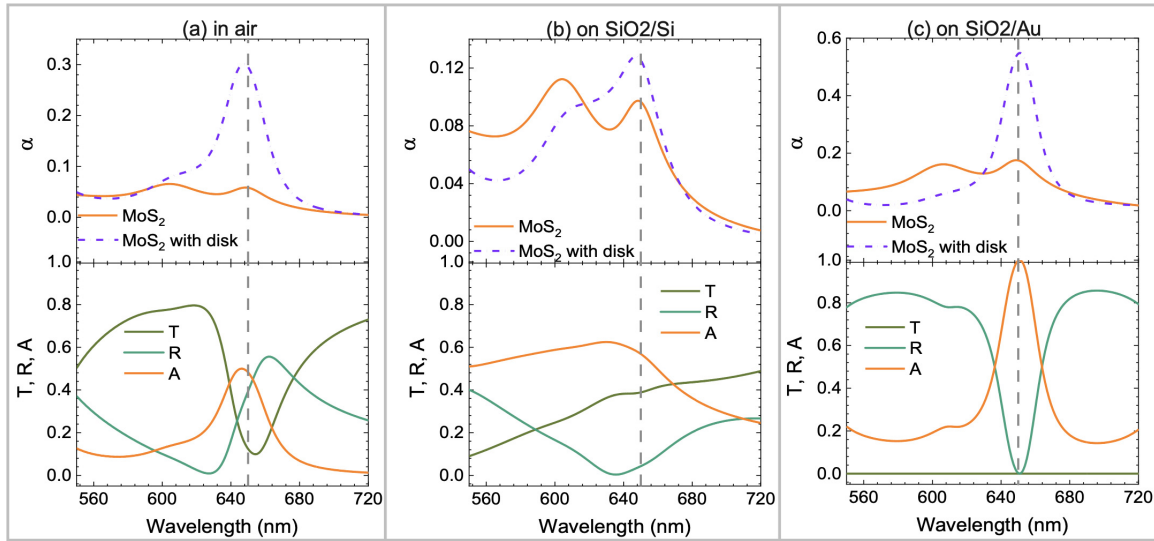


FIG. 3. The separate MoS₂ monolayer and the hybrid MoS₂-monolayer-disk structures are examined for three cases: (a) in air, (b) on SiO₂/Si substrate, and (c) on SiO₂/Au substrate, respectively. The disk has radius $r = 150$ nm, height $h = 45$ nm, and spacer thickness $s = 100$ nm. Top panels: the absorbance of the MoS₂ monolayer in the alone and hybrid cases. Bottom panels: the reflectance R , transmittance T , and absorbance A of the total structure.

dipole \mathbf{P} and electric toroidal dipole contributions \mathbf{Te} , as well as the magnetic quadrupole \mathbf{M} , are dominant in the far-field reflectance or transmittance. The magnetic dipole \mathbf{m} and electric quadrupole \mathbf{Q} are negligible. Higher-amplitude multipolar modes are seen for the disk resonator on SiO₂/Au substrate, which results from the higher generated electric field amplitude within the disk resonator compared with that in air or on SiO₂/Si substrate. Since the dominant multipo-

lar modes, including the total electric dipole and magnetic quadrupole, have the same even parity in the forward and backward scattering plane [33,35], the scattering profile does not depend on the incidence port, along z or $-z$. Under the incident light along z , the forward scattering (z) is reflected by the gold mirror, which is incident on the disk resonators again, resulting in the other forward ($-z$) and backward scattering (z). Both scattering generated by the incident light

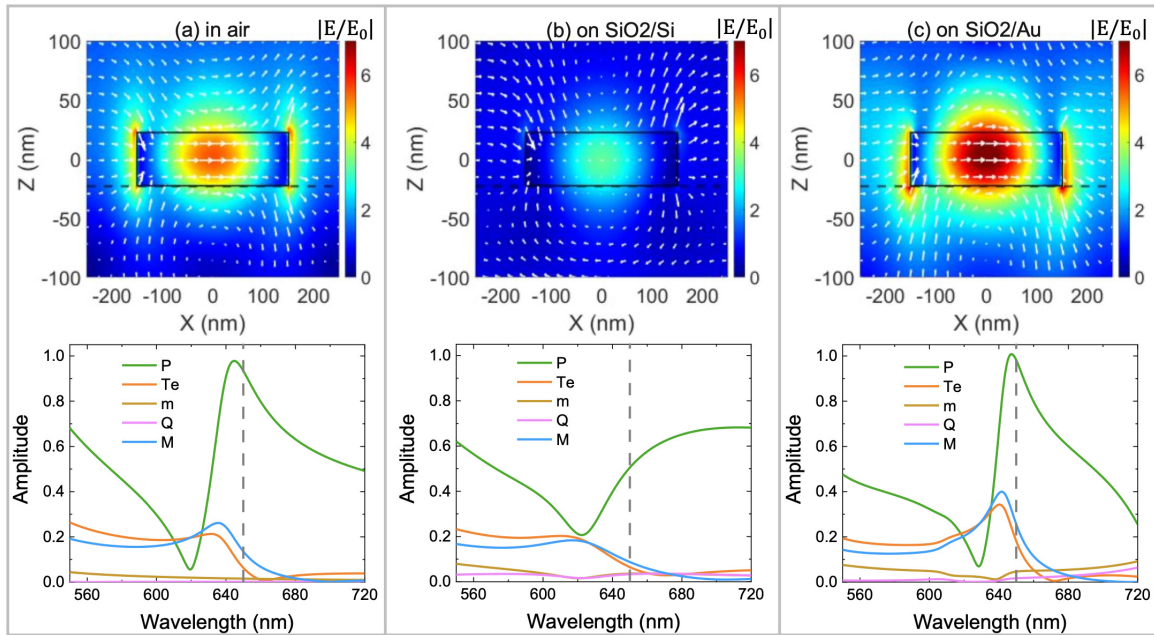


FIG. 4. (a)–(c) Top panels: the simulated amplitude ratio of the electric field, $|E/E_0|$, in the x - z plane at $y = 0$ at the inspected absorbance wavelength of 646 nm. The disk has radius $r = 150$ nm, height $h = 45$ nm, and spacer thickness $s = 100$ nm. The black dashed line illustrates where the MoS₂ monolayer is, and the incident light propagates along the $+z$ direction. Bottom panels: the amplitude of the multipolar modes for reflectance and transmittance coefficients, including the electric dipole \mathbf{P} , electric toroidal dipole \mathbf{Te} , magnetic dipole \mathbf{m} , electric quadrupole \mathbf{Q} , and magnetic quadrupole \mathbf{M} .

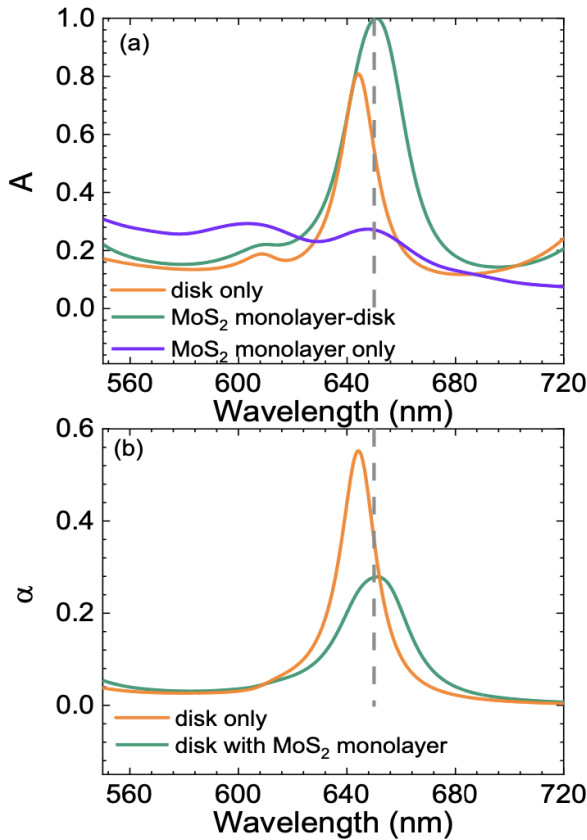


FIG. 5. (a) Comparison of the absorbance A of the structures on SiO₂/Au substrate for disk radius $r = 150$ nm, height $h = 45$ nm, and spacer thickness $s = 100$ nm, including the disk only, the monolayer MoS₂ only, and the hybrid monolayer MoS₂-disk. (b) The absorbance α of the Si nanodisk only on SiO₂/Au substrate as well as the Si nanodisk in the hybrid monolayer MoS₂-disk on SiO₂/Au substrate.

and gold mirror reflection superimpose coherently. This corresponds well with the observation of near-identical spectral line shapes for the decomposed multipolar modes of the disk resonators on SiO₂/Au substrate compared with those for the structure suspended in air [Figs. 4(a) and 4(c)], only with different amplitudes, indicating that the gold plane plays the role of a second input port. Fabry-Pérot-type multiple reflections are also present; however, these can be treated as negligible [34,36]. Moreover, due to the constraint of power conservation in the cases of the perfect absorber and partial

absorber, it is interesting to explore the effect of monolayer MoS₂ on the absorbance of disk resonators. From Fig. 5(a), it can be seen that when the absorbance of the alone monolayer MoS₂ directly on the SiO₂/Au substrate is almost resonant with that of the disk resonators, the absorbance of the hybrid structure shows a redshift due to the high imaginary permittivity of monolayer MoS₂. Furthermore, as can be seen in Fig. 5(b), the absorbance of the Si nanodisks is reduced in the hybrid case, and the resonance redshifts due to the presence of monolayer MoS₂. This indicates that the incident energy redistributes in the hybrid structures, driven by relative imaginary permittivity of the disk and the monolayer MoS₂ as well as the modified electric field distributions within the disk and monolayer MoS₂, respectively, compared with those for each separate element.

IV. CONCLUSION

In conclusion, the optical absorbance of monolayer MoS₂ on an array of Si disk nanoresonators is explored experimentally and theoretically. Emission enhancement is experimentally observed for MoS₂ on the nanodisk array. This is due to increased absorbance in the MoS₂ monolayer, which also compensates for emission quenching due to the presence of the disk. The model explains the observed emission enhancement and is used to further explore increasing the magnitude of the absorbance of monolayer MoS₂ using Si nanodisk resonators. With the aid of the gold mirror, a perfect absorbing structure is proposed, where the incident power is totally absorbed by the hybrid monolayer MoS₂-Si disk resonators. The dominant total electric dipole including toroidal dipole contributions as well as the magnetic quadrupole drive the resonant absorbance enhancement. By analyzing the absorbance of the disk resonator and monolayer MoS₂, respectively, it is seen that the full electromagnetic power is redistributed within the hybrid structures compared with those for the separate components. The absorbance of monolayer MoS₂ is enhanced while the absorbance of disk resonators is reduced. Moreover, compared with a monolayer MoS₂ suspended in air, where the absorbance value of the A exciton peak value is smaller than 10%, a value of more than 50% is achieved in the perfect absorbing structures.

ACKNOWLEDGMENTS

We wish to acknowledge the support of Science Foundation Ireland (SFI) under Grants No. 16/IA/4550 and No. 17/NSFC/4918.

- [1] L. Novotny and B. Hecht, *Principles of Nano-Optics* (Cambridge University Press, Cambridge, 2012).
- [2] S. Ogawa, M. Imada, S. Yoshimoto, M. Okano, and S. Noda, *Science* **305**, 227 (2004).
- [3] Z. Wang, Z. Dong, Y. Gu, Y.-H. Chang, L. Zhang, L.-J. Li, W. Zhao, G. Eda, W. Zhang, G. Grinblat, S. A. Maier, J. K. W. Yang, C.-W. Qiu, and A. T. S. Wee, *Nat. Commun.* **7**, 11283 (2016).
- [4] K. Aoki, D. Guimard, M. Nishioka, M. Nomura, S. Iwamoto, and Y. Arakawa, *Nat. Photonics* **2**, 688 (2008).
- [5] S. Kühn, U. Håkanson, L. Rogobete, and V. Sandoghdar, *Phys. Rev. Lett.* **97**, 017402 (2006).
- [6] A. F. Koenderink, *ACS Photonics* **4**, 710 (2017).
- [7] B. Zhao, J. Zhao, and Z. Zhang, *J. Opt. Soc. Am. B* **32**, 1176 (2015).
- [8] J. Le Perchec, *Opt. Lett.* **44**, 590 (2019).

- [9] E. M. Purcell, H. C. Torrey, and R. V. Pound, *Phys. Rev.* **69**, 37 (1946).
- [10] M. Khajavikhan, A. Simic, M. Katz, J. Lee, B. Slutsky, A. Mizrahi, V. Lomakin, and Y. Fainman, *Nature (London)* **482**, 204 (2012).
- [11] F. Xia, T. Mueller, Y.-m. Lin, A. Valdes-Garcia, and P. Avouris, *Nat. Nanotechnol.* **4**, 839 (2009).
- [12] T. Jiang, D. Huang, J. Cheng, X. Fan, Z. Zhang, Y. Shan, Y. Yi, Y. Dai, L. Shi, K. Liu, C. Zeng, J. Zi, J. E. Sipe, Y.-R. Shen, W.-T. Liu, and S. Wu, *Nat. Photonics* **12**, 430 (2018).
- [13] K. F. Mak, C. Lee, J. Hone, J. Shan, and T. F. Heinz, *Phys. Rev. Lett.* **105**, 136805 (2010).
- [14] J. R. Piper, V. Liu, and S. Fan, *Appl. Phys. Lett.* **104**, 251110 (2014).
- [15] H. Lu, X. Gan, D. Mao, Y. Fan, D. Yang, and J. Zhao, *Opt. Express* **25**, 21630 (2017).
- [16] H. Li, M. Qin, L. Wang, X. Zhai, R. Ren, and J. Hu, *Opt. Express* **25**, 31612 (2017).
- [17] S. Butun, S. Tongay, and K. Aydin, *Nano Lett.* **15**, 2700 (2015).
- [18] T. Galfsky, Z. Sun, C. R. Consideine, C.-T. Chou, W.-C. Ko, Y.-H. Lee, E. E. Narimanov, and V. M. Menon, *Nano Lett.* **16**, 4940 (2016).
- [19] X. Zhang, S. Choi, D. Wang, C. H. Naylor, A. C. Johnson, and E. Cubukcu, *Nano Lett.* **17**, 6715 (2017).
- [20] E. Palacios, S. Park, L. Lauhon, and K. Aydin, *ACS Photonics* **4**, 1602 (2017).
- [21] S. Butun, E. Palacios, J. D. Cain, Z. Liu, V. P. Dravid, and K. Aydin, *ACS Appl. Mater. Interfaces* **9**, 15044 (2017).
- [22] Y. Chong, L. Ge, H. Cao, and A. D. Stone, *Phys. Rev. Lett.* **105**, 053901 (2010).
- [23] D. G. Baranov, A. Krasnok, T. Shegai, A. Alù, and Y. Chong, *Nat. Rev. Mater.* **2**, 17064 (2017).
- [24] W. Li, A. G. Birdwell, M. Amani, R. A. Burke, X. Ling, Y.-H. Lee, X. Liang, L. Peng, C. A. Richter, J. Kong, D. J. Gundlach, and N. V. Nguyen, *Phys. Rev. B* **90**, 195434 (2014).
- [25] See Supplemental Material at <http://link.aps.org/supplemental/10.1103/PhysRevMaterials.6.045202> for details about (a) reflectance and photoluminescence measurements, (b) Raman measurements of monolayer MoS₂, (c) the comparison between reflectance measurements and simulation, and (d) theoretical quantification of photoluminescence enhancement; the Supplemental Material includes Refs. [37,38].
- [26] J. D. Jackson, *Classical Electrodynamics*, 3rd ed. (Wiley, New York, 1999).
- [27] G. Baffou, R. Quidant, and C. Girard, *Appl. Phys. Lett.* **94**, 153109 (2009).
- [28] B. Zhao, J. Zhao, and Z. Zhang, *Appl. Phys. Lett.* **105**, 031905 (2014).
- [29] K.-H. Brenner, *Opt. Express* **18**, 10369 (2010).
- [30] L. Sortino, P. Zotev, S. Mignuzzi, J. Cambiasso, D. Schmidt, A. Genco, M. Aßmann, M. Bayer, S. Maier, R. Sapienza, and A. I. Tartakovskii, *Nat. Commun.* **10**, 5119 (2019).
- [31] M. M. Fogler, S. Yang, A. T. Hammack, L. V. Butov, and A. C. Gossard, *Phys. Rev. B* **78**, 035411 (2008).
- [32] C. Zhang, H. Wang, W. Chan, C. Manolatou, and F. Rana, *Phys. Rev. B* **89**, 205436 (2014).
- [33] A. B. Evlyukhin, T. Fischer, C. Reinhardt, and B. N. Chichkov, *Phys. Rev. B* **94**, 205434 (2016).
- [34] X. Zhang, J. Li, J. F. Donegan, and A. L. Bradley, *Phys. Rev. Materials* **4**, 125202 (2020).
- [35] X. Zhang and A. L. Bradley, *Phys. Rev. B* **103**, 195419 (2021).
- [36] V. E. Babicheva, M. I. Petrov, K. V. Baryshnikova, and P. A. Belov, *J. Opt. Soc. Am. B* **34**, D18 (2017).
- [37] C. Lee, H. Yan, L. E. Brus, T. F. Heinz, J. Hone, and S. Ryu, *ACS Nano* **4**, 2695 (2010).
- [38] H. Li, Q. Zhang, C. C. R. Yap, B. K. Tay, T. H. T. Edwin, A. Olivier, and D. Baillargeat, *Adv. Funct. Mater.* **22**, 1385 (2012).